Surface stress and shape relaxation of gelling droplets – Supporting information - SI

J. Godefroid, D. Bouttes, A. Marcellan, E. Barthel and C. Monteux

September 2023

1 Flow curves of the alginate suspensions

The flow curve of the alginate suspension is obtained using an AR-G2 rheometer from TA instruments using a cone plate geometry with a steel cone of 40 mm diameter and 2 degrees angle.

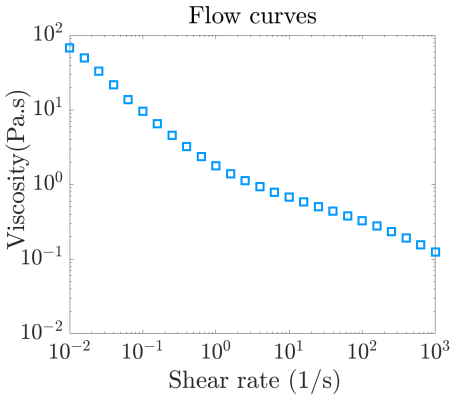

Figure 1: Rheology curve of the alginate solution used to produce the droplets

We first use a pre-shear step where an intense pre shear at 1000 s-1 is

applied for 60 seconds to all samples prior to the shear flow curve measurement.

2 Mechanical properties of the alginate hydrogels

The goal of the compression experiments is to determine an order of magnitude of the compression modulus of the alginate-zirconia hydrogels.

We perform the compression tests on flat gel cylinders of 10 mm diameter and 4 mm in height with an Instron tensile meter using a flat tool of 2 cm of diameter. To obtain the cylinders we pour a beaker with an alginate zirconia suspension and then add a calcium solution on top of the solution to trigger the solidification. After two weeks we remove the hydrogel cylinder out of the beaker. We chose this time as the mechanical properties tend to vary over time and stabilize after two weeks toward a reproducible measurement. To obtain the desired diameter we use a round cutter. Moreover to ensure a good planeity of our samples, we use a razor blade to obtain a flat surface. Indeed the hydrogel tends to get curved during the solidification process. The stress strain curve presented below enables to obtain a rough estimation of the order of magnitude of the elastic modulus of the order of 25 kPa. If the gel cylinder was purely elastic one would expect a linear variation of the stress with the applied strain which is not the case. We suspect that for small strains the sample unperfect flatness disturbs the measurement. At larger strains we expect that plastic deformation might lead to a non linear

relation between stress and strain.

We note that the measurements presented below are performed on hydrogel aged of two weeks, which is probably much higher than the modulus of the gelled layer a few seconds after the droplets enter in the calcium bath. The results probably largely overestimate the value of the elastic modulus of the freshly gelled layer of the droplets falling into the bath. In the article we arbitrarily take a value of the elastic modulus of the order of 10 kPa to estimate the tensile stress in the gelling layers.

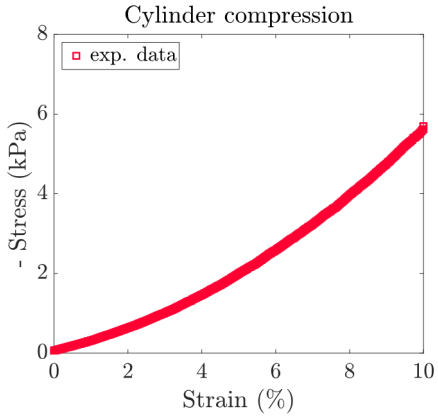

Figure 2: Stress strain curves of the alginate hydrogels

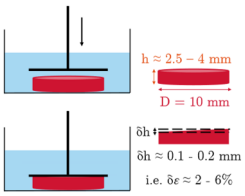

Figure 3: schematic drawing explaining how we perform the mechanical measurements

3 Mass loss of the alginate beads

The goal of this section is to obtain a rough estimation of the weight loss of the alginate beads as a function of the calcium concentration. We dripped our suspension in a bath of calcium and weighed the beads as a function of time until a steady state is reached. As shown below we find that the mass of water expelled is of the order of 10 to 15 percent.

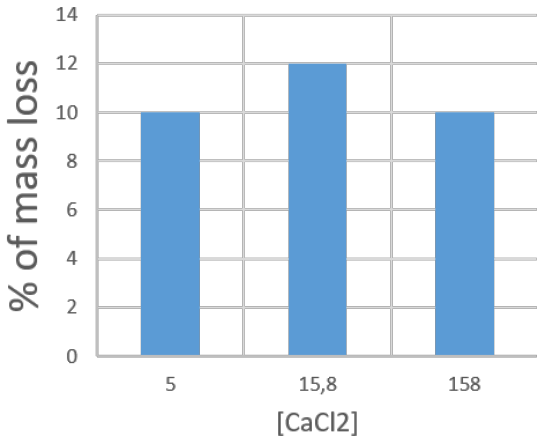

Figure 4: Mass loss of the alginate hydrogels due to syneresis

4 Experimental relaxation of the suspension droplets in an immiscible oil - non gelling case

We performed a number of experiments in a non reacting and immiscible medium, oil. A typical relaxation curve is shown in Fig. 4.

Interestingly the droplet aspect ratio varies exponentially over time even-though the droplets suspensions are a non Newtonian fluid. The droplet relaxation time that we find experimentally, around 40 ms, is consistent with

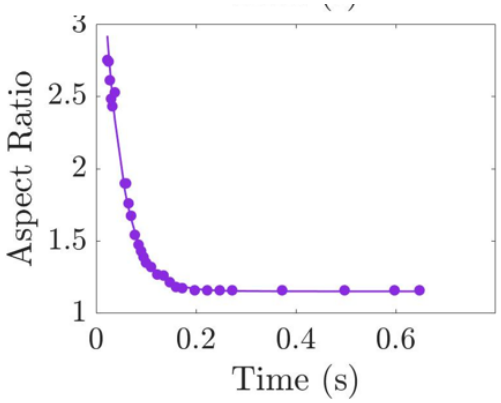

Figure 5: Droplet relaxation in an oil bath. The relaxation is exponential with a characteristic time $t_{rel} = 0.04$ s.

a viscosity $\eta \approx$ 1 Pa.s, taking the oil/water interfacial tension of $\gamma \approx 0,03$ N/m that we measured independently. As the suspensions are shear thinning fluids, their viscosity decreases with the shear rate. A viscosity $\eta \approx$ 1 Pa.s-1 found from the aspect ration relaxation time corresponds to a shear rate $\dot{\gamma} \approx 100$ s-1. This value is consistent with the impact shear rate defined as $\dot{\gamma} \approx U/D \approx 100$ s-1, with $U \approx 1$ m/s the impact velocity and $D \approx 1$ mm the diameter of the drop. $\dot{\gamma}$ represents the shear rate in the drop during the impact, assuming no slip conditions at the drop/bath interface. This result means that the restructuration time of the fluid is longer than the relaxation time of the drops and that the viscosity of the suspensions does not have time to rise after the impact.

5 Numerical model

A lagrangian description of the displacement field is convenient because both elasticity and free surfaces are readily included. Numerical solutions were

obtained with the finite elements technique (Abaqus [1]). The model is two dimensional, *i.e.* we perform a plane strain calculation with an initially elliptic cross section relaxing towards a circular cross section.

5.1 Constitutive equation of the material

The liquid core is modeled as a linear viscoelastic solid with a negligible long time elastic shear modulus μ_∞ and a relaxation time $\tau = \eta/\mu_0$ where η is the viscosity and μ_0 the short time elastic shear modulus. This description is efficient because moderate deformations are involved. For the material constitutive relation, we take a simple exponential relaxation with a characteristic time τ

$$\bar{\bar{\sigma}}_{dev}(t) = \mu_0 \int_0^t \exp\left(\frac{t-t'}{\tau}\right) \frac{d\bar{\bar{\epsilon}}_{dev}(t')}{dt'} dt' \tag{1}$$

where $\bar{\bar{\sigma}}$ and $\bar{\bar{\epsilon}}$ denote the stress and strain tensors, the subscript dev the deviatoric parts.

In Abaqus the constitutive relation Eq. 1 can be obtained with viscoelasticity treated as a one-term Prony series (*Viscoelastic, time = PRONY) and the requested material properties are the short time Young's modulus $E_{t=0}$, the parameter $g = 1 - (E_{t=\infty}/E_{t=0})$ and the relaxation time τ. To determine $E_{t=0}$ we use the relation $\mu_0 = E_{t=0}/3$. In that scheme, we need to ensure negligible initial elastic strains and negligible final elastic stresses: since the stress level is of the order of $\gamma/R \simeq 1$, we typically take $E_{t=0} = 300$, $\tau = 0.01$ and $g = 0.9999$. The material is nearly incompressible in the liquid phase ($\nu = 0.499$).

5.2 Numerical scheme for the gelling droplets

We introduce a scalar field $\mathcal{C}$ representing the Ca^{2+}concentration. At the surface of the droplet we keep $\mathcal{C}$ constant equal to the concentration of the bath $\mathcal{C}_{bath}$ while inside the droplet, $\mathcal{C}$ is initially zero. In the numerical scheme, the initial bath concentration is applied through a fast but smooth step at $t = 0$. Calcium diffusion is allowed inside the droplet following a Fickian law

$$\frac{\partial \mathcal{C}}{\partial t} = \kappa \Delta \mathcal{C} \tag{2}$$

where κ is the diffusion coefficient. For that purpose, the most straightforward strategy is to map the Ca^{2+} concentration $\mathcal{C}$ to the temperature field (element type CPE4HT), using $\mathcal{C}$ values of the order of unity. Calcium diffusion is implemented through standard heat diffusion (*Conductivity). The temperature field obeys $c_p \rho \frac{dT}{dt} = \nabla \cdot (\kappa_T \nabla T)$ where c_p is the specific heat, ρ the density and κ_T the thermal conductivity. Numerically, we take $c_p = \rho = 1$ and take the thermal conductivity κ_T numerically equal to the Ca^{2+} diffusion coefficient κ.

To model the gelation process itself, *i.e.* the transformation of the Newtonian liquid into an elastic solid under the action of Ca^{2+}, we let the relaxation time of the Maxwell fluid *increase* steadily with calcium concentration $\mathcal{C}$, keeping the short time elastic modulus μ_0 constant. Such a slowing down of the dynamics is a situation commonly encountered for materials undergoing a glass transition from high to low temperatures. Following standard approaches used to describe this transition [1] we introduce a local time $\xi(t)$, the so called reduced time, which *decreases* sharply with the calcium con-

centration. More precisely we use the integral equation:

$$\xi(t) = \int_0^t \frac{ds}{A(\mathcal{C}(s))} \tag{3}$$

with t the simulation time and A a shift factor which varies with the concentration through the simple phenomenological relation

$$\log\left(A(\mathcal{C})\right) = \beta\mathcal{C} \tag{4}$$

β sets the concentration for which the material has effectively become a solid. For a concentration $\mathcal{C} \simeq 1$, $\beta = 10$ results in a reduction of the actual time by a factor 10^{-10} or alternatively a 10^{10} increase of the relaxation time. The relaxation time being then much larger than the total simulation time, the material effectively behaves as an elastic solid with a shear modulus given by the instantaneous modulus μ_0. Following our numerical scheme, in Abaqus we use the standard WLF relation (*Trs) with TRS parameters 0, -1000, 100, closely approximating Eq. 4. We also ensure that gelification decreases the Poisson ratio to 0.4 (linear with $\mathcal{C}$): this evolution has been included for consistency with the idea of transformation into a solid but it is not expected to have a strong impact on the relaxation process.

Finally we also need to model the contraction $\epsilon_{\mathcal{C}}$ of the material due to syneresis: it is accounted for by applying an isotropic material strain proportional to the Ca^{2+} concentration. The contraction coefficient is taken as α. The order of magnitude of the eigenstrain can be estimated from volumetric shrinkage $\frac{1}{3}\delta V/V_0$ based on the measured macroscopic volume loss

$\delta V/V_0 \approx 15\%$. Note also that we have introduced a saturation concentration $\mathcal{C}_{sat}$ above which no more contraction is incurred. We use this saturation concentration to normalize the concentrations so that we will use $\mathcal{C}_{sat} = 1$. This saturation creates a sharper gelation front at concentrations $\mathcal{C} > \mathcal{C}_{sat}$. As explained in the main text, this saturation concentration is a key element to qualitatively reproduce all the experimental observations. The strain induced by the Ca^{2+} (so called eigenstrain) is given by

$$\epsilon_{\mathcal{C}} = \alpha\, \mathcal{C} \quad \text{for} \quad \mathcal{C} < \mathcal{C}_{sat} \tag{5}$$

$$\epsilon_{\mathcal{C}} = \alpha\, \mathcal{C}_{sat} \quad \text{for} \quad \mathcal{C} \geq \mathcal{C}_{sat} \tag{6}$$

with $\alpha = -0.1$. Roughly speaking, in the gelled layer, $\epsilon_{\mathcal{C}} = -0.1$. For our numerical scheme, we developed a simple user function UEXPAN (in incremental form).

An example model file is included (E3SB_Conc_AR_2_small_mod_1p5.inp) with the user routine uexpan1x_sat.f for thermal expansion with saturation at unit concentration. The model file also calls the file AR_2_small_mod.inp which contains the geometry, the mesh, the surfaces and the sets for an initial aspect ratio of 2.5.

5.3 Simulation of the capillary relaxation of an elongated droplet without gelation

We first calculate the relaxation of this purely Newtonian elongated ellipse under the action of surface tension γ (Fig 7). For that purpose, surface

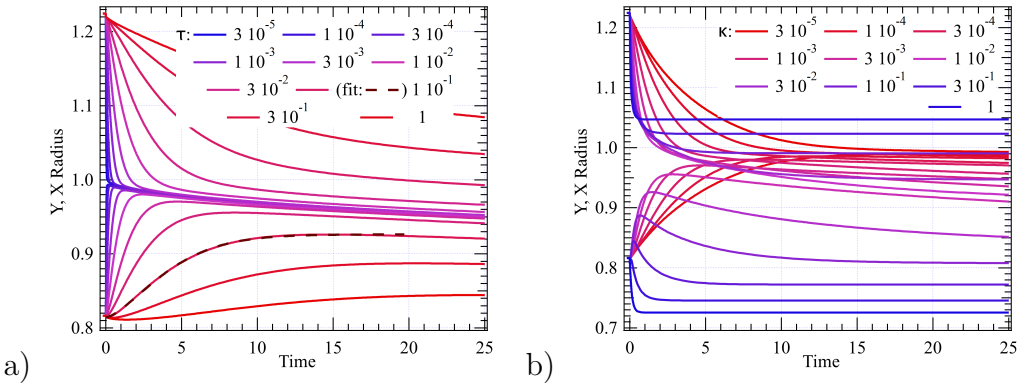

Figure 6: plots of R_X and R_Y *vs.* time showing the impact of the material relaxation time τ (a - $\kappa = 0.001$) and diffusion coefficient κ (b - $\tau = 0.01$) on droplet relaxation for $\mathcal{C}_{bulk} = 1$ and an initial aspect ratio 1.5. A fit to a non exponential relaxation with exponent 1.45 is also shown (dashed black line)

tension elements are applied to the free surface, following references [2, 3]. The initial cross section is elliptic with $R_X = \sqrt{3}$, $R_Y = 1/\sqrt{3}$ *i.e.* an aspect ratio $AR = 3$. The material parameters are $\gamma = 1.0$ and $\eta = 1.0$ and time is normalized by the material relaxation time τ. A typical evolution of the ellipse shape and the associated pressure distributions are shown in Fig. 7a with three successive configurations. The time evolution of the aspect ratio and pressure gradients are plotted in Fig 7b and Fig 7c. It is seen that the ellipse relaxes towards a circle with radius $R_X = R_Y = 1$, *i.e.* the final aspect ratio $AR = 1$. The time evolution of the radii is exponential with a characteristic time of

$$t_c = \eta R/\gamma \tag{7}$$

corresponding to the classical capillary relaxation time for Newtonian liquids [4, 5]. The pressure distribution clearly evidences a higher pressure at the apex having the smallest radius of curvature, as expected from a Laplace

pressure. The pressure gradient is the driving force for the liquid flow leading to relaxation towards a circular shape (Fig 7c). All these results fully match the expected behaviour for a Newtonian viscous liquid under the action of surface tension, validating the numerical scheme.

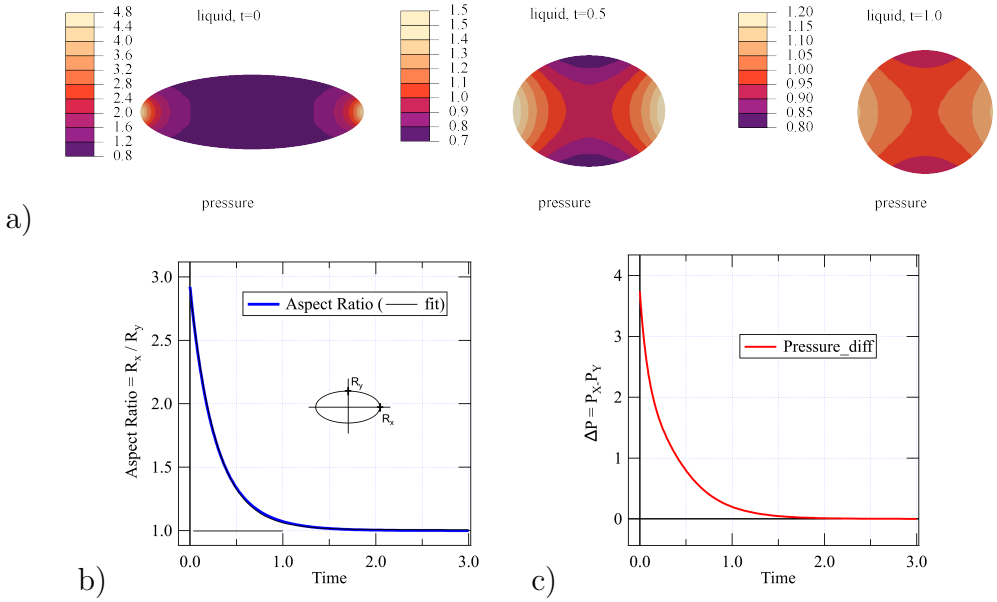

Figure 7: Numerical results for the relaxation of a viscous liquid under the action of surface tension. a) Representative snapshots of the elongated droplets relaxation for $\eta = 1$ and $\gamma = 1$ at t=0, t=0.5 and t=1.0. The pressures at the apices R_x and R_y are also displayed b) time evolution of the aspect ratio. An exponential fit (small dashes - black), as predicted by small strain analytical calculations, is almost indistinguishable from the numerical result. c) Pressure gradient as a function of time

5.4 Numerical results of gelling drops

To test the model, series of results were calculated for an initial aspect ratio of 1.5, $\mathcal{C}_{bath} = 1$ and a range of values of τ and κ. The evolution of R_X and R_Y with time for $\kappa = 0.001$ and varying τ is shown in Fig. 6 a. We observe the expected slowing down of the droplet relaxation process as τ (or the

viscosity η) increases. Similar results varying the diffusion coefficient κ are shown in Fig. 6 b. The general evolution of the radii with time is affected by a decrease of the diffusion coefficient κ in a manner which is roughly similar to an increase in the relaxation time τ.

The evolution of the aspect ratio for different relaxation times and different diffusion coefficients is shown in Fig. 8 where the time axis has been rescaled. The curves collapse, demonstrating the validity of the approximate model. In fact, for equal $\kappa\tau$ products, identical evolutions are obtained provided time has been rescaled. This result is to be expected: in fact, since Ca^{2+} diffusion (Eq. 2) is independent from the droplet deformation, and because the strains incurred are moderate, it only provides time dependent boundary conditions (under the form of eigenstrain field) from which the solution to the evolution equation is computed. It would require extreme deformations for geometrical effects to impact diffusion and thus couple the equations. Since τ and κ play inverse roles in the time scales involved (see *e.g.* Eq. **??** with $\eta = \mu\tau$), there is effectively only one time parameter in the calculation.

In Fig. 6 a, the non-exponential behaviour of the relaxation can be observed as an inflection in the early stages of the relaxation. It is especially clear for the larger values of the relaxation time and for the small (Y) radius. As shown by the analytical results (Eq. 6 in the main text), this inflection results from the increasing driving force incurred through the growth of the surface stress layer, in contrast to the constant surface tension for the non reactive oil-gel interface. Fits to the results in Fig. 6 are adequate when the exponent is allowed to deviate from 1.5. For the different cases shown the

exponent varies between 1.2 and 1.7. The difference from the predicted value 1.5 originates from the rather simplified representation of the surface layer used to obtain Eq. 4 (main text) and to geometrical non linearities.

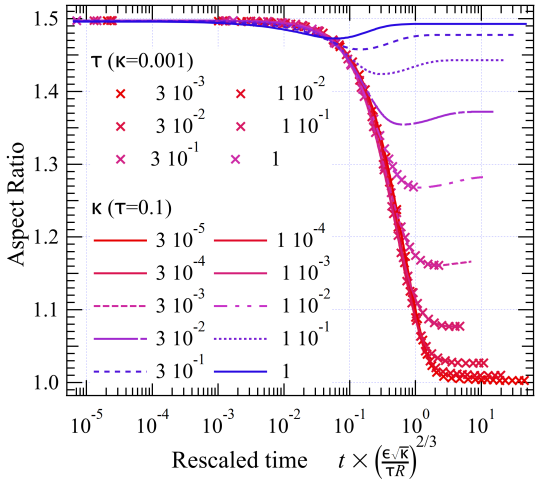

Figure 8: Impact of relaxation time and diffusion coefficient on droplet relaxation for $\mathcal{C}_{bulk} = 1$ and an initial aspect ratio 1.5. Note that that once rescaled, identical curves are obtained for equal $\kappa\tau$ ratios (see text).

As shown in the main text, the ultimate stage of the relaxation does not follow the same scaling : waiting longer when the viscosity is large is not the same as waiting for a short time when viscosity is moderate because at longer times bending resistance steps in due to increasing thickness of the gelled layer. To test the prediction of the approximate analytical model (Eq. **??** in the main text), we calculated relaxation curves with R_X=3 and R_Y=1 and $\mathcal{C}_{bulk} = 1$, for different values of the diffusion coefficient. The results are shown in Fig. 9 a. The transition is particularly visible in the downturn which appears in the Y radius at large diffusion coefficient values. This downturn reflects material contraction. In the aspect ratio plots (Fig. 9 b), this downturn is reflected with a minimum and when, following Eq.**??**,

time is rescaled by κ, the minima fall at a nearly constant position of the order of ϵ (Fig. 9 right). This result confirms our scaling approach.

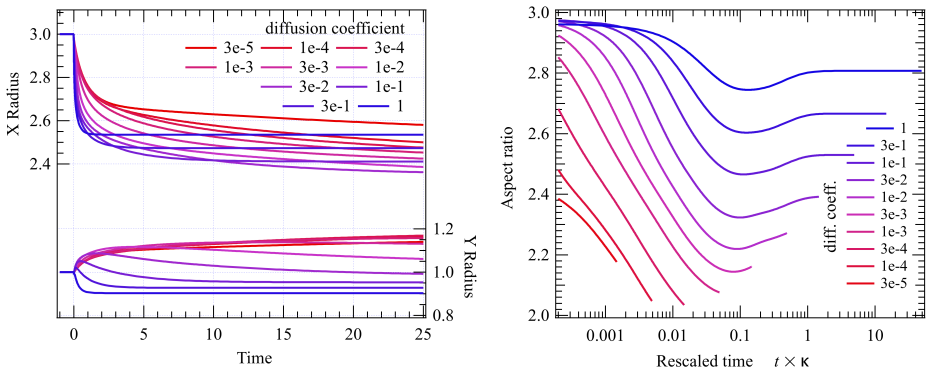

Figure 9: plots of R_X and R_Y *vs.* time showing the impact of the diffusion coefficient on the shape relaxation process. Rescaled following Eq. **??**, the transitions, marked by a dip, all collapse.

References

[1] *Abaqus reference manual*. HKS, Providence, 2016.

[2] A Jagota, C Argento, and S Mazur. Growth of adhesive contacts for maxwell viscoelastic spheres. *Journal of applied physics*, 83(1):250–259, 1998.

[3] Robert W Style, Anand Jagota, Chung-Yuen Hui, and Eric R Dufresne. Elastocapillarity: Surface tension and the mechanics of soft solids. *Annual Review of Condensed Matter Physics*, 8:99–118, 2017.

[4] Dominique Barthès-Biesel. Capsule motion in flow: Deformation and membrane buckling. *Comptes Rendus Physique*, 2009.

[5] Jérémie Teisseire, Amélie Revaux, Maud Foresti, and Etienne Barthel. Confinement and flow dynamics in thin polymer films for nanoimprint lithography. *Applied Physics Letters*, 98(1):013106, 2011.